Electronic Supplementary Material (ESI) for Journal of Materials Chemistry A.
This journal is © The Royal Society of Chemistry 2023

Supplementary Information

Ultrahigh Energy Storage Capacity in Multilayer-Structured Cellulose-Based Dielectric Capacitors Caused by Interfacial Polarization-Coupled Schottky Barrier Height

Zixiong Sun[a,b,c,d,e], Jiaqi Liu[b], Hansong Wei[b], Qing Guo[a], Yuhan Bai[a], Shibo Zhao[a], Siting Wang[a], Lei Li[f], Yutao Zhang[f], Ye Tian[f], Xiaohua Zhang[f], Hongmei Jing[g], Yongping Pu[f], Sufeng Zhang[b]**

a School of Electronic Information and Artificial Intelligence, Shaanxi University of Science and Technology, Xi'an 710021, PR China

b Shaanxi Provincial Key Laboratory of Papermaking Technology and Specialty Paper Development, National Demonstration Center for Experimental Light Chemistry Engineering Education, Key Laboratory of Paper Based Functional Materials of China National Light Industry, Shaanxi University of Science and Technology, Xi'an, 710021, PR China

c Key Laboratory of Auxiliary Chemistry and Technology for Chemical Industry, Ministry of Education, Shaanxi University of Science and Technology, Xi'an 710021, PR China

d Shaanxi Collaborative Innovation Center of Industrial Auxiliary Chemistry and Technology, Shaanxi University of Science and Technology, Xi'an 710021, China

e MESA$^+$ Institute for Nanotechnology, University of Twente PO Box 217, 7522 NH Enschede, The Netherlands

f School of Materials Science and Engineering, Shaanxi University of Science and Technology, Xi'an 710021, PR China

g School of Physics and Information Technology, Shaanxi Normal University, Xi'an, 710119, PR China

**Corresponding author: Zixiong Sun, Sufeng Zhang*

E-mail address: SunZX@sust.edu.cn, zhangsufeng@sust.edu.cn

Experimental Section

Materials

The cellulose comes from the cotton linter purchased from Hubei Jinhuan New Material Technology Co., Ltd. The DMAc (99.0%), LiCl (99.0%), PVDF (average Mw~534,000 $gmol^{-1}$), and the barium titanate (BT, 99.0%) were all purchased from Sinopharm Chemical Reagent Co., Ltd. The diameter of BT particles is around 100 nm.

Fabrication of the $BaTiO_3$@cellulose/PVDF precursors

The fabrication process of the $BaTiO_3$@cellulose/PVDF precursors follows the technology of our previous work[1]. The cellulose was first activated in DMAc aqueous solution by being stirred at 160 ^oC for 30 min, after which the cellulose was lifted out and put in the LiCl aqueous solution with the mass ratio of cellulose(s)/DMAc(l)/LiCl(s) equals to 2/51/5. The obtained solution needed to be stirred again at 100 ^oC for 3 hours, then the transparent cellulose solution was obtained after standing for another 24 hours. Meanwhile, the PVDF solution was obtained after a 6-hour stirring of the mixture of PVDF(s), DMAc(l), and LiCl(s) (3:51:5 by mass) at 50 ^oC. The two kinds of solutions were then mixed with a mass ratio of cellulose/PVDF equal to 80/20, and the BT particles were added afterward with the volume fraction of 0%, 2/3%, 5/3%, 2%, 5%, 8%, and 10%, respectively. All the ternary solutions with different BT content must be stirred for at least 12 h until they were mixed uniformly. Finally, a 30-minute ultrasonic concussion-assisted magnetic stirring with the repetition of 5 times was carried out on them to obtain the $BaTiO_3$@cellulose/PVDF precursors with different BT content.

Fabrication of multilayers with different structures and BT contents.

Multilayers can be fabricated using the precursors obtained above through the tape-casting method. Unlike conventional technology, in our work, every *next layer* of the multilayer was cast before the *previous layer* was completely dry. By doing so, the interaction of the hydrogen bond network, which is more active in a liquid environment, between adjacent layers helped to form the multilayered structure and flattened the interfaces. The authors would like to emphasize here that this procedure has little scientific problem behind it but might need many attempts to determine the best moment for casting the *next layer*. Here, we fabricated two kinds of structures: the uniform-structured multilayers with every sub-layer having the same BT content and the sandwich-structured ones with the out layers of C8P2 and the inner layer of $BaTiO_3$@cellulose/PVDF(C8P2-BT) with different BT contents. The sandwich-structured multilayers with the middle layer having the BT content of 0%, 2%, 5%, 8%, and 10% in volume fraction are written as 0-0-0, 0-2-0, 0-5-0, 0-8-0, and 0-10-0, respectively. In contrast, the two uniform-structured multilayers have the same BT content as 0-2-0 and 0-5-0, so every sub-layer has a BT content of 2/3% and 5/3% in volume fraction, respectively.

Characterization

The crystalline structure of all the multilayers was measured by X-ray diffraction (XRD *Rigaku D/max-2200PC*). The Microstructures for surface morphologies, cross-sections, and lattice fringe of BT particles were measured by scanning electron microscope(SEM *Thermo Fisher Scientific*) and transmission electron microscopy (FE-TEM, *JEOL, JEM-F200*). The Fourier transform infrared spectroscopy (FTIR, *Spotlight 400 & Frontier*) was employed to identify the functional groups of multilayers. Before electric properties' measurements, electrodes with diameters of 1 mm were sputtered on both sides of the films. Both the frequency dependence of the dielectric constant(ε) with dielectric loss($tan\delta$) and temperature dependence of the dielectric constant(ε) with dielectric loss($tan\delta$) were obtained from the impedance analyzer(*E4980A, Agilent*). The *J-E* curves and hysteresis loops(*P-E* loops) were measured using a ferroelectric tester(*Radiant Premier II*), and the measuring frequency for the *P-E* loops is 100 Hz. The dynamic discharging performances were obtained from a charging-discharging measurement system(*Tongguo technology, CFD-003, China*) with a load resistance of 100 Ω.

The servo control system universal testing machine (*AI-7000-NGD, Gotech Testing Machines*) was employed for measuring the mechanical properties.

According to the *Rietveld* method, the *FullProf* was used for the XRD refinement. The original CIF card was chosen from the previous literature[2].

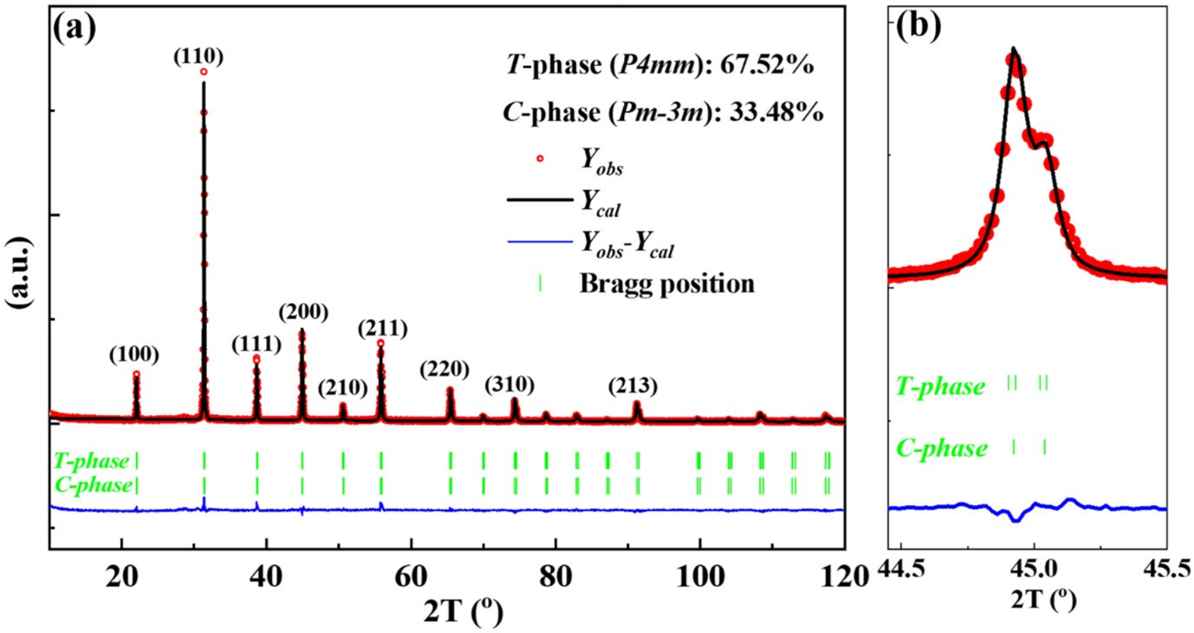

Fig. S1 (a) The XRD pattern and its Rietveld refinement result from 0° to 120° of BT used in this work. (b) The enlarged view from 44.4° to 45.5° of Fig. S1(a), and the (002) peak split can be observed.

Tab. S1 The lattice parameters with c/a ratio and lattice volume derived from the Rietveld refinement process of the BT particles in this work.

Material	**Lattice parameters (Å)**	***c/a***	**Volume (Å^3)**	**R_{wp} (%)**	**R_p (%)**	**χ^2 (%)**
BaTiO$_3$	***C*** (67.52%) *a*=4.0164	1.000	64.790	9.79	9.31	3.53
	T (33.48%) *a*=*b*=4.0128, *c*=4.0213	1.002	64.753			

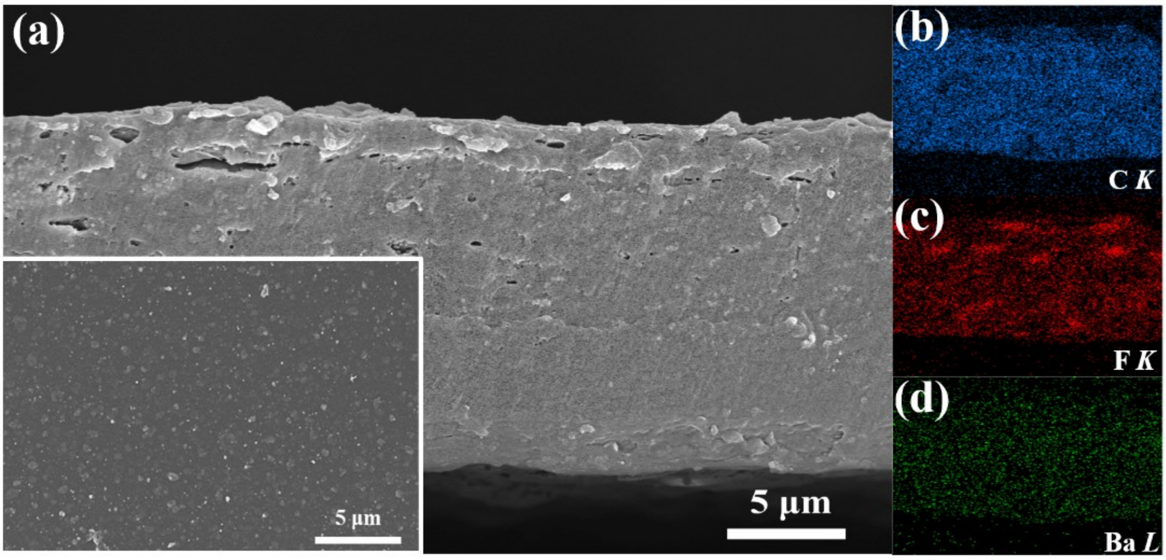

Fig. S2 (a) The SEM cross-section image of the 2/3-2/3-2/3 and the image for the surface morphology is inserted on the left bottom; (b)-(d) EDS mappings for C, F, and Ba, respectively, of 2/3-2/3-2/3.

Wei-bull Distribution

Before calculating the energy storage density(ESD), the electric breakdown strength(E_b) of each film should be confirmed by employing the *Weibull* distribution, which can be expressed as follow[3,4]:

$$X_i = \ln E_\mathrm{i} \qquad \text{Eq. S1}$$

$$Y_i = \ln (- \ln (1 - P_\mathrm{i})) \qquad \text{Eq. S2}$$

$$P_i = \frac{i}{1+n} \qquad \text{Eq. S3}$$

where X_i and Y_i are the two parameters of the Weibull distribution, Y_i varies linearly with X_i with a slope of β, $E_{i,}$ and P_i are the sample's breakdown field and the electric field's failure probability distribution, respectively. While n, i, and β are the total number of specimens, the serial number of dielectric strength, and the slope of the linear relationship between $\ln(E_i)$ and $\ln(-\ln(1-P_i))$, respectively.

Calculation of ESD and η

The ESD and η of a dielectric capacitor under a specific applied electrical field (E) can be represented by the following formula[1]:

$$W_{\mathrm{rec}} = \int_{P_{\mathrm{m}}}^{P_{\mathrm{r}}} E\mathrm{d}P \qquad \text{Eq. S4}$$

$$W_{\mathrm{char}} = \int_{0}^{P_{\mathrm{m}}} E\mathrm{d}P \qquad \text{Eq. S5}$$

$$\eta = W_{rec}/W_{sto}100\% \qquad \text{Eq. S6}$$

The W_{rec} and $W_{char,}$ are the ESD and energy-charged density(ECD) during one charge-discharge process, respectively. P is the generated polarization under E, and the P_m and P_r are the maximum polarization upon charging and the remanent polarization when the electrical field returns to zero, respectively.

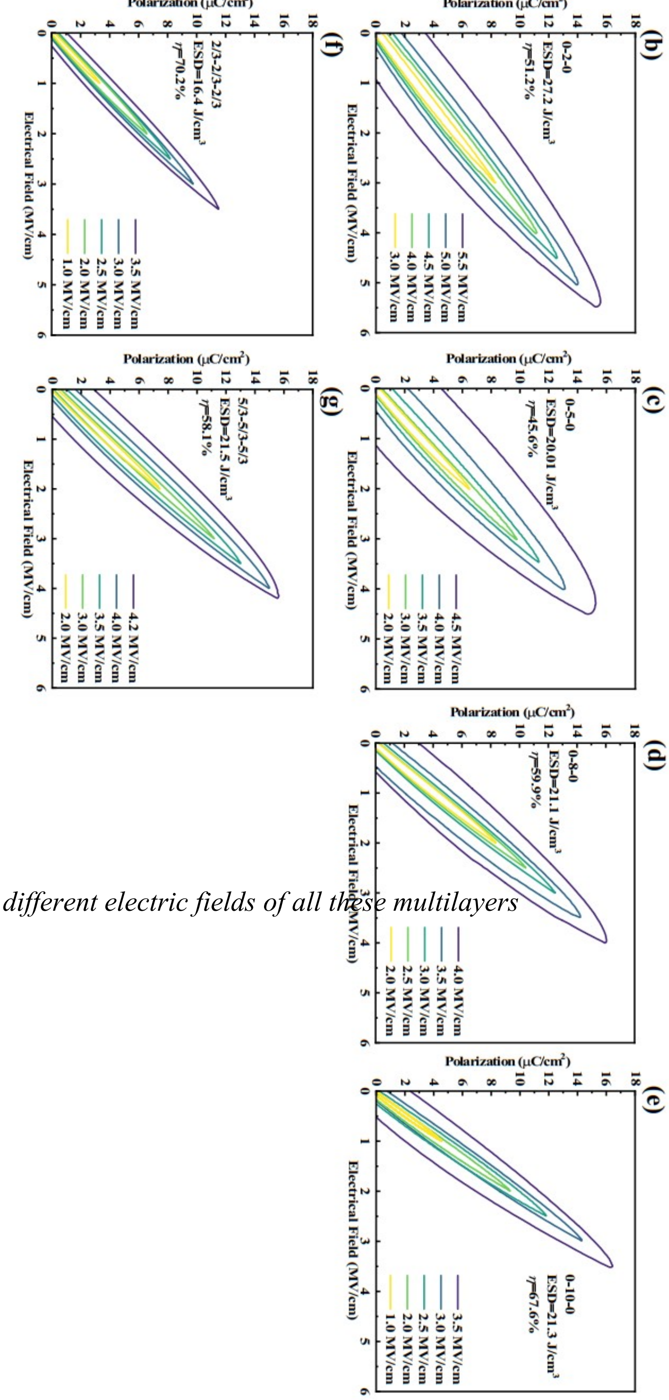

Fig. S3 The unipolar P-E loops at different electric fields of all these multilayers

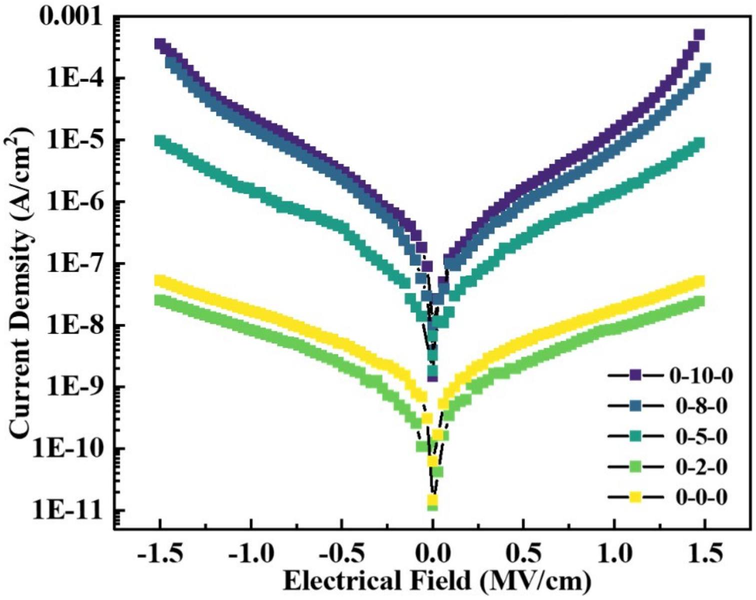

Fig. S4 The J-E curves of the sandwich-structured multilayers

The physical meaning of the abbreviations in the band diagram analyzing

E_{VAC}: the vacuum level

E_{FA}: the Fermi energy level of Au

E_{FC}: the Fermi energy level of C8P2

E_{CC}: the conduction band of C8P2

E_{VC}: the valence band of C8P2

E_{FB}: the Fermi energy level of BT

E_{CB}: the conduction band of BT

E_{VB}: the valence band of BT

ϕ_A: the work function of Au

ϕ_C: the work function of C8P2

χ_C: the electron affinity of C8P2

ϕ_S: the Schottky barrier height

ϕ_b: the build-in potential

V_b: the applied bias

ϕ_{Vb}: the barrier height caused by the V_b

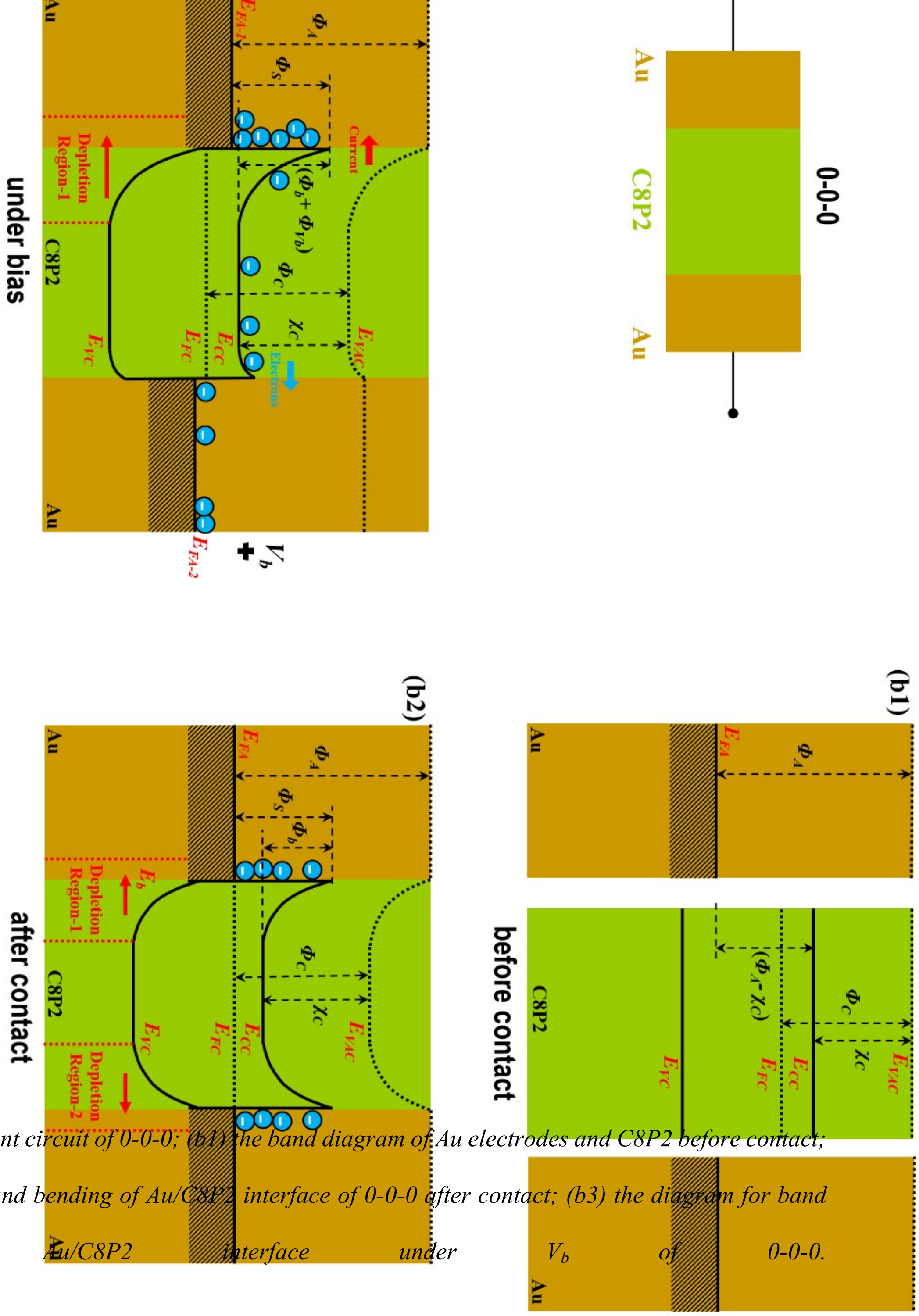

Fig. S5 (a) The equivalent circuit of 0-0-0; (b1) the band diagram of Au electrodes and C8P2 before contact; (b2) the diagram for band bending of Au/C8P2 interface of 0-0-0 after contact; (b3) the diagram for band bending of Au/C8P2 interface under V_b of 0-0-0.

Fig. S6 (a) and (b) shows the *P-E* loops of 0-0-0, 0-2-0, and 0-8-0 measured under 4.5 MV/cm.at 1Hz and 5 Hz, respectively. Two conclusions can be extracted in such a comparison: (1) the polarization of *P-E* loops for the capacitors with higher BT content is higher than that with lower BT content, which is because of the much higher polarization of BT than C8P2. (2) The polarization in capacitors with higher BT content drops more slowly than that with lower BT content, and this can be attributed to the interfacial polarization, which is a kind of relaxor polarization and occurs between the BT particles and the C8P2 matrix.

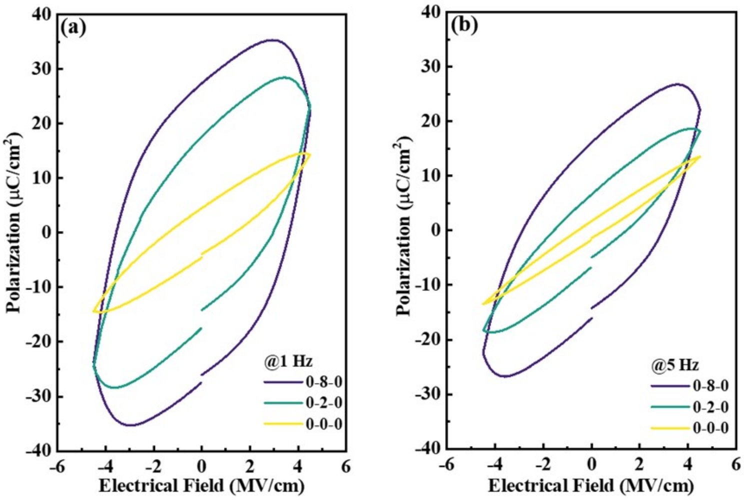

Fig. S6 P-E loops of 0-0-0, 0-2-0, and 0-8-0 at (a) 1Hz and (b) 5 Hz under 4.5 MV/cm.

Finite Element Simulation

The *COMSOLMultiphysics6.0* was employed for the simulation of the current spread.

The electrical breakdown process was described according to the spread of current density. Boundary conditions should meet

$$\boldsymbol{n}\cdot\boldsymbol{i}=0 \qquad \text{Eq. S7}$$

where $\boldsymbol{n}$ and $\boldsymbol{i}$ are the normal and current density vectors, respectively. This boundary condition means that no electric current flows into the. The constitutive relations are expressed as follows:

$$\boldsymbol{J}=\sigma\boldsymbol{E} \qquad \text{Eq. S8}$$

which is the standard *Ohm's law* and

$$\boldsymbol{D}=\varepsilon_0\varepsilon_r\boldsymbol{E} \qquad \text{Eq. S9}$$

where $\boldsymbol{J}$ and $\boldsymbol{E}$ are the current density and external electrical field, respectively, and σ and ε_r are each material's electrical conductivity and dielectric constant (permittivity), which needs input in the model. ε_0 is vacuum permittivity with a value of $8.854187817*10^{-12}$ F/m. Considering the stationary equation of continuity of the model after a long time, Eq. S5 should be changed to a more general form:

$$\boldsymbol{J}=\sigma\boldsymbol{E}+\frac{\partial\boldsymbol{D}}{\partial t}+\boldsymbol{J_e} \qquad \text{Eq. S10}$$

At the same time, current conservation should be met from then on with the equations:

$$\nabla\cdot\boldsymbol{J}=Q_{j.v} \qquad \text{Eq. S11}$$

$$\boldsymbol{E}=-\nabla V \qquad \text{Eq. S12}$$

where $Q_{j.v}$ and $\boldsymbol{D}$ represent the change rate of electric charge per unit volume and the electric displacement vector. The $\boldsymbol{J_e}$ is the current density and density of the external electric current, and V denotes the electrical potential. The University of Twente offers the serial number of *COMSOLMultiphysics 6.0.*

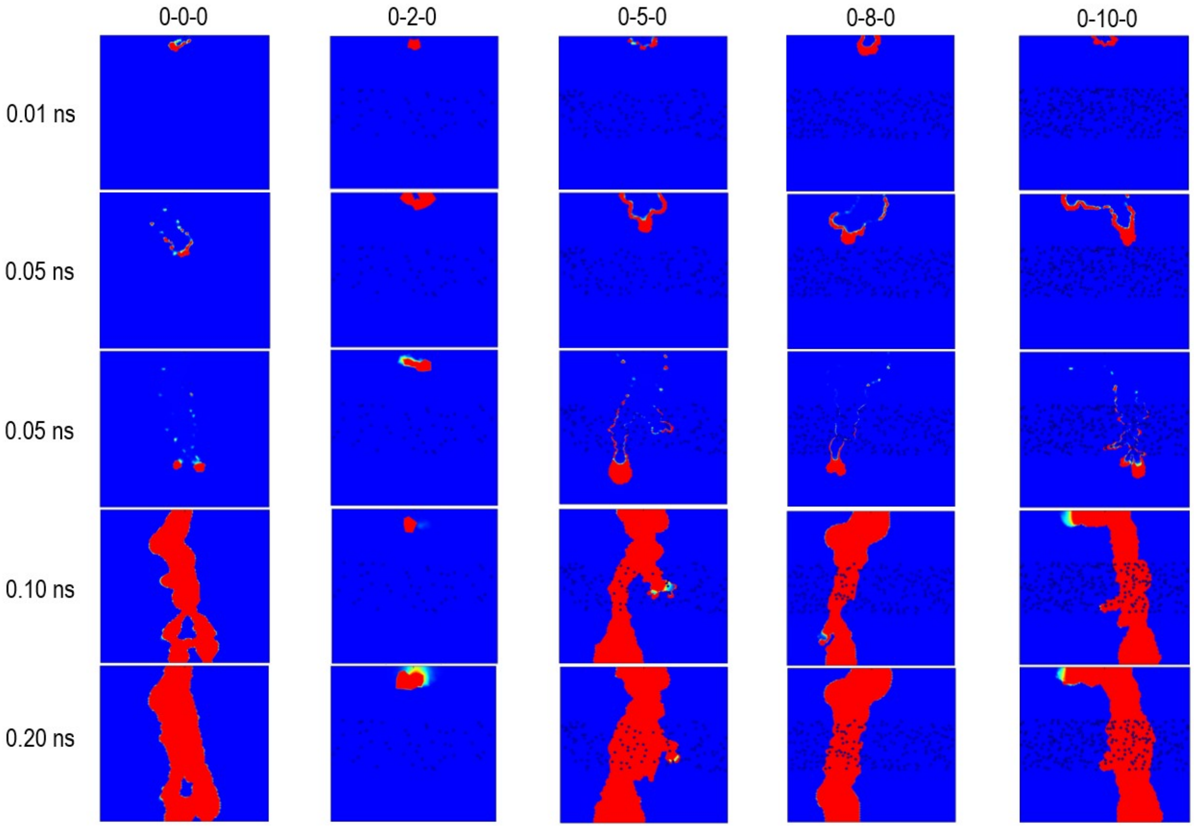

Fig. S7 The spread of current density at different times of all the sandwich-structured multilayers under 5.3 MV/cm.

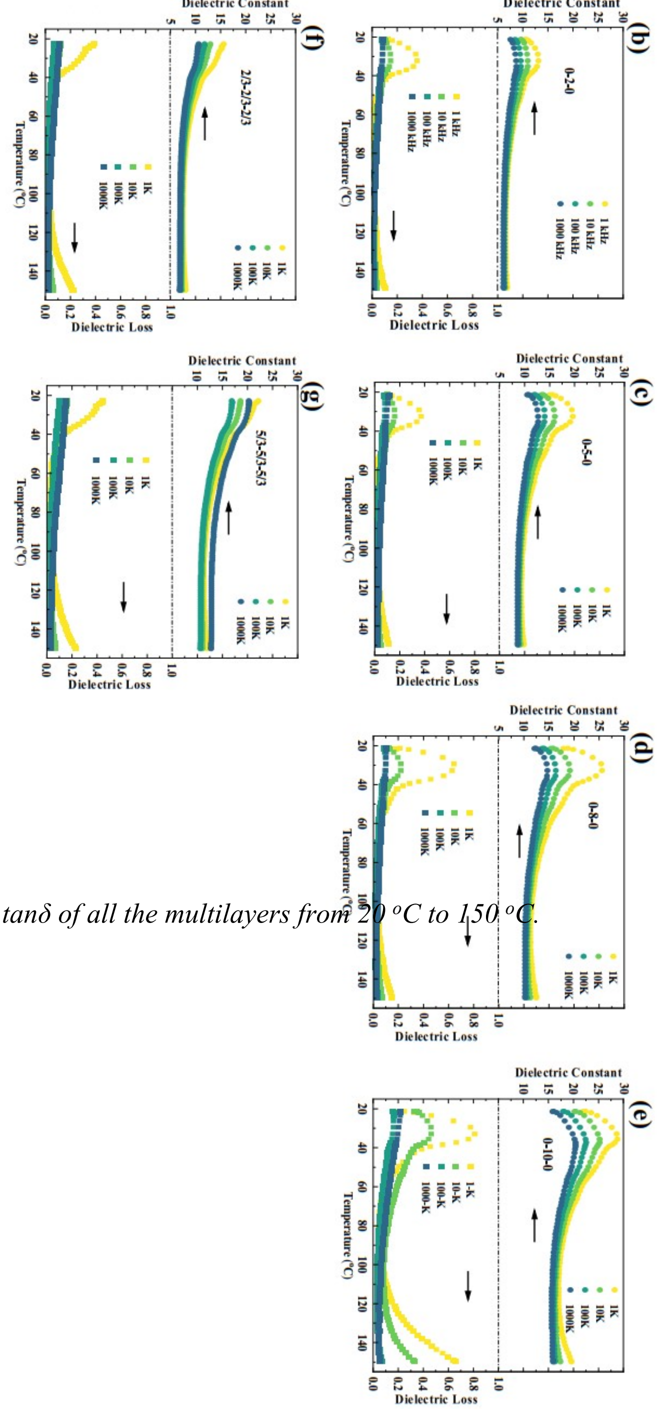

Fig. S8 The temperature dependence of the ε and tanδ of all the multilayers from 20 °C to 150 °C.

The electric field distribution of 2/3-2/3-2/3 and 0-2-0

Before analyzing, we define the uniform structure of 2/3-2/3-2/3 as condition-1 and the sandwich structure of 0-2-0 as condition-2, respectively. The sketches of both structures are displayed in Fig. S9(a1) and (a2), respectively, and Fig. S9(b1) and (b2) show their corresponding equivalent circuits. Because the BT particles disperse uniformly in 2/3-2/3-2/3, the equivalent circuit can be regarded as two capacitors representing BT and C8P2 matrix, connecting in series. Each capacitor's partial voltage and thickness are written as U_{C8P2-1}, U_{BT-1}, and d_{C8P2-1}, d_{BT-1}, respectively. For 0-2-0, things are complicated. Its equivalent circuit can also be considered as two capacitors connected in series, but the two capacitors are defined as C8P2 and C8P2-BT, which represents the outer layers and the middle layer, respectively. Similar to condition-1, the C8P2-BT can also be seen as BT and C8P2 connecting in series, as illustrated in Fig. S9(b3). In Fig. S9(b2), each capacitor's partial voltage and thickness are written as U_{C8P2-2}, $U_{C8P2-BT-2}$, and d_{C8P2-2}, $d_{C8P2-BT-2}$, respectively. In Fig. S9(b3), each capacitor's partial voltage and thickness are written as U_{C8P2-2}', U_{BT-2}, and d_{C8P2-2}', d_{BT-2}, respectively.

After applying the same voltage (U) in both multilayers, we can have the relationship of

$$Q_{C8P2-1} = Q_{BT-1} \qquad \text{Eq. S13}$$

in 2/3-2/3-2/3 and

$$Q_{C8P2-2} = Q_{C8P2-BT-2} \qquad \text{Eq. S14}$$

in 0-2-0, respectively, in which the Q_{C8P2-1}, Q_{BT-1} and Q_{C8P2-2}, $Q_{C8P2-BT-2}$ are the charge in C8P2, BT in condition-1 and the charge in C8P2, BT in condition-2, respectively. When the equilibrium is reached, the following equation will be established,

$$Q1 = Q_{C8P2-1} = Q_{BT-1} \qquad \text{Eq. S15}$$

$$Q2 = Q_{C8P2-2} = Q_{C8P2-BT-2} \qquad \text{Eq. S16}$$

in which the Q_1 and Q_2 are the total charge in 2/3-2/3-2/3 and 0-2-0, respectively. The relationship between Q, U, and C, the relationship between E, U, and d, and the definition of C is expressed as:

$$Q = UC \qquad \text{Eq. S17}$$

$$C = \frac{\varepsilon S}{4k\pi d} \qquad \text{Eq. S18}$$

$$U = Ed \qquad \text{Eq. S19}$$

where the C, E, ε, S, d, and k are the capacitance of the capacitor, the electric field of the capacitor under U, the dielectric constant of the dielectric layer, the overlapped area of the two electrodes, the thickness of the dielectric and the Boltzmann constant, respectively.

By combining Eq. S9, Eq. S11, Eq. S12 and Eq. S13, in condition-1, we can have

$$\frac{E_{BT-1}}{E_{C8P2-1}} = \frac{\varepsilon_{BT}}{\varepsilon_{C8P2}} \qquad \text{Eq. S20}$$

Where the E_{BT-1} and E_{C8P2-1} are the electric fields on BT and C8P2, respectively, and the ε_{BT-1} and ε_{C8P2-1} are the corresponding dielectric constant. Eq. S14 tells that the electric field applied on each layer in 2/3-2/3-2/3 is inversely proportional to their dielectric constant.

By combining Eq. S10-S13, in condition-2, we can have:

$$\frac{U_{C8P2-BT-2}}{U_{C8P2-2}} = \frac{\varepsilon_{C8P2-2}}{\varepsilon_{C8P2-BT-2}} \cdot \frac{d_{C8P2-BT-2}}{d_{C8P2-2}} \qquad \text{Eq. S21}$$

in which the ε_{C8P2-2} and $\varepsilon_{C8P2-BT-2}$ are the dielectric constant of the out layer and middle layer of 0-2-0, respectively. The ε_{C8P2-2} should be the dielectric constant of pure C8P2 matrix but the value of $\varepsilon_{C8P2-BT-2}$ is missing, so we fabricated a film with the same BT content as the middle layer in 0-2-0. After carrying out the C-V measurement, as displayed in Fig. S10, the ε_{C8P2-2} and $\varepsilon_{C8P2-BT-2}$ at 2.0 MV/cm are 2.5 and 3.2, respectively. Considering equations as follows,

$$d = \frac{3}{2} d_{C8P2-2} = 3 d_{C8P2-BT-2} \qquad \text{Eq. S22}$$

$$U = U_{C8P2-2} + U_{C8P2-BT-2} \qquad \text{Eq. S23}$$

we can have

$$U_{C8P2-BT-2} = 0.4U \qquad \text{Eq. S24}$$

Because the voltage distribution of BT and C8P2 in the middle layer of condition-2 also follows Eq. S14, the voltage applied on BT particles in condition-2 is only 0.4 times that in condition-1. Normally, the polarization is proportional to the applied field, which follows the equations as follows:

$$P = \chi e \varepsilon 0 E \qquad \text{Eq. S25}$$

In which the χ_e called electric susceptibility and the ε_0 is the vacuum permittivity. The polarization induced by the BT particles in 0-2-0 is also only 0.4 times that in 2/3-2/3-2/3. Compared to the C8P2 matrix, BT particles contribute the most polarization in our composite due to their large dipole moment. For the whole multilayers, under the same voltage, the polarization of 2/3-2/3-2/3 should be higher than that of 0-2-0.

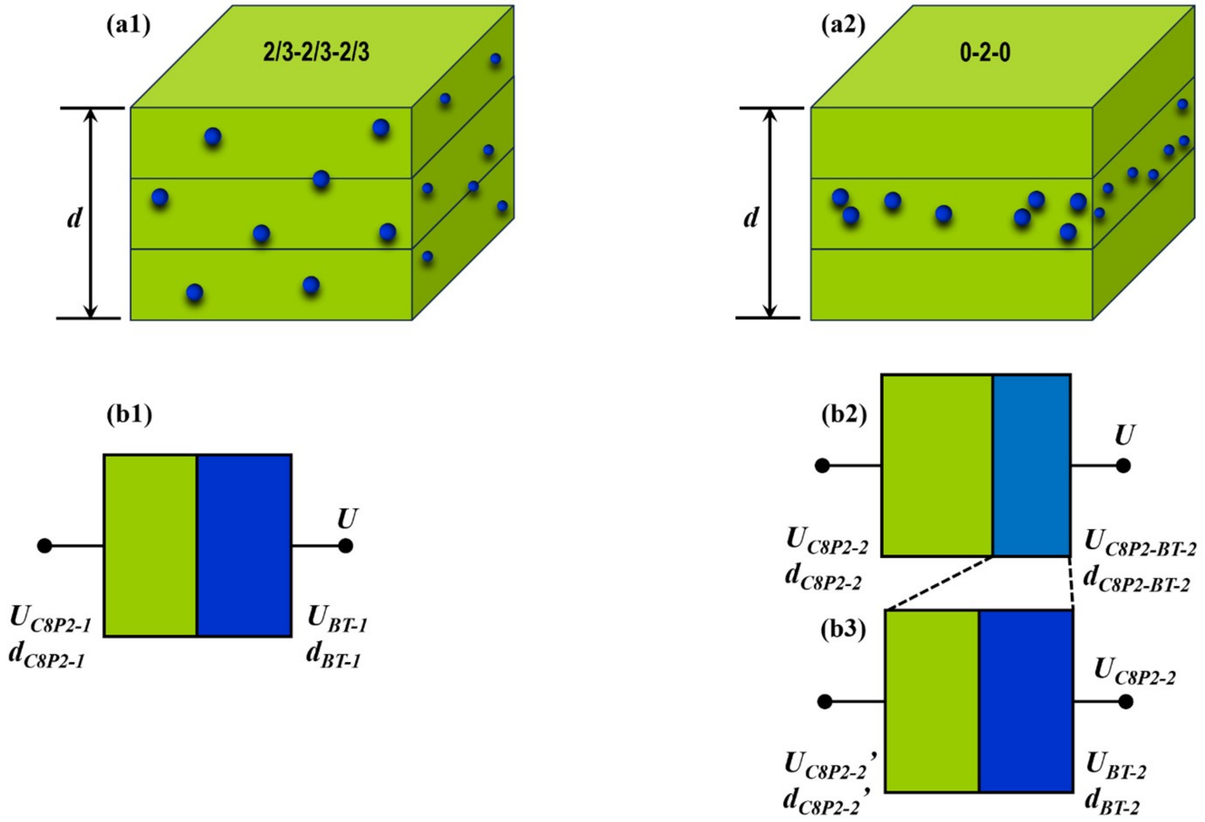

Fig. S9 Schematic of (a1) 2/3-2/3-2/3; (b) 0-2-0; schematic of the double-layer mode of (b1) 2/3-2/3-2/3; (b2) 0-2-0; (b3) middle layer of 0-2-0

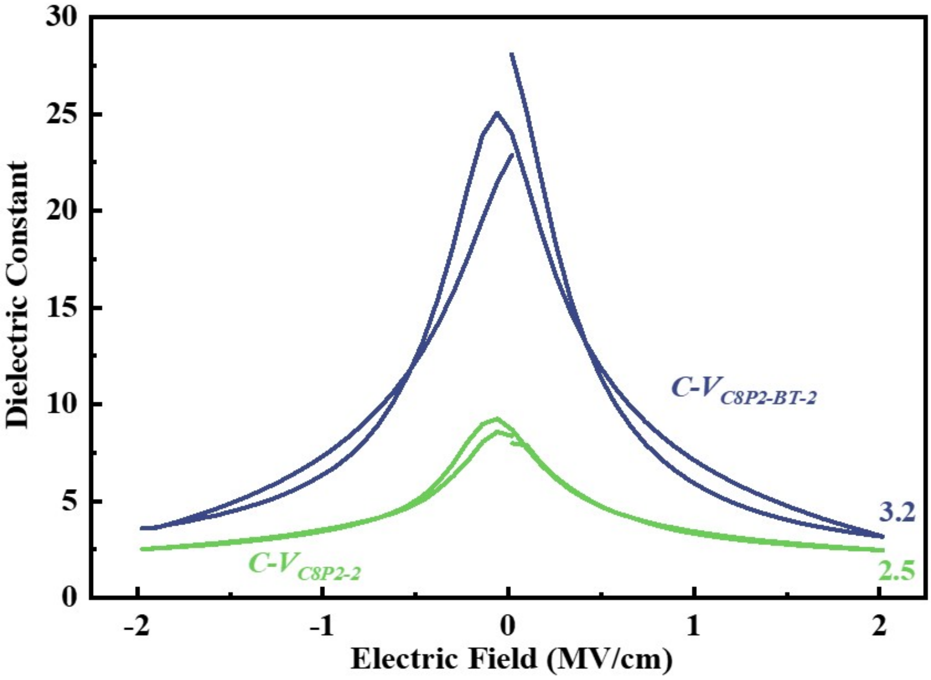

Fig. S10 Schematic of (a1) 2/3-2/3-2/3; (b) 0-2-0; schematic of the double-layer mode of (b1) 2/3-2/3-2/3; (b2) 0-2-0; (b3) middle layer of 0-2-0.

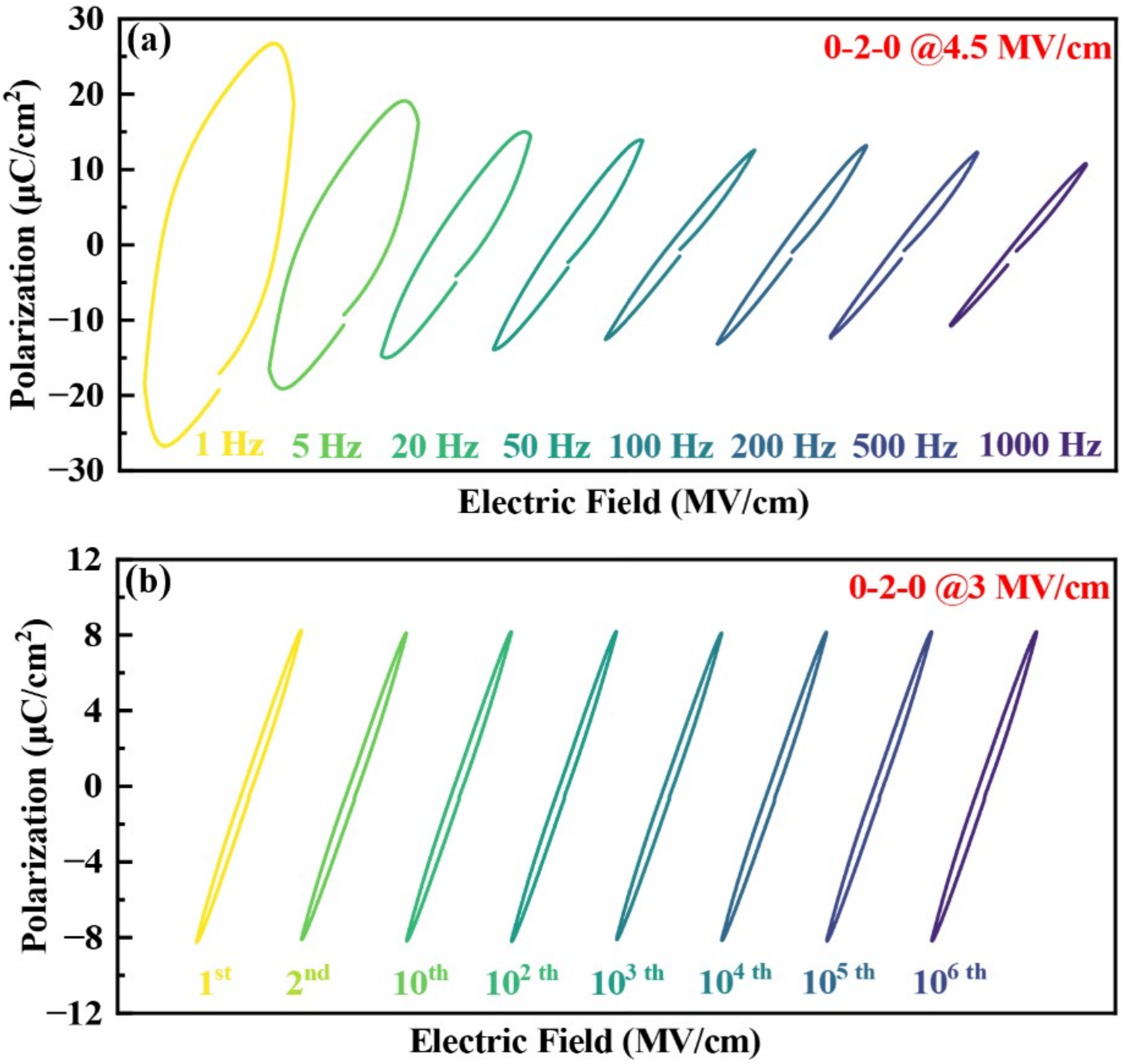

Fig. S11 (a) P-E loop of 0-2-0 measured from 1 Hz to 1000 Hz at 4.5 MV/cm; (b) P-E loop of 0-2-0 measured at 3 MV/cm during the polarization fatigue process from the 1st cycle to the 10^{6th} cycle.

References

[1] S. Zhang, J. Liu, Q. Guo, N. Wei, Y. Ning, Y. Bai, Y. Tian, T. Wang, Z. Sun, Y. Pu, *Composites, Part A.*, 2023, **165**, 107329.

[2] G. H. Kwei, A. C. Lawson, S. J. L. Billinge, S. W. Cheong, *J. Phys. Chem.* **1993**, 97, 10, 2368-2377

[3] Y. Huan, T. Wei, X. Wang, X. Liu, P. Zhao, X. Wang, *Chem. Eng. J.*, 2021, **425**, 129506.

[4] L. Liu, Y. Liu, J. Hao, J. Chen, P. Li, S. Chen, P. Fu, W. Li, and J. Zhai, *Nano Energy*, 2023, **109**, 108275.